11th International Conference on Vibration Problems
Z. Dimitrovová *et.al.* (eds.)
Lisbon, Portugal, 9–12 September 2013

OBTAINING INERTIAL AMPLIFICATION INDUCED PHONONIC GAPS VIA STRUCTURAL OPTIMIZATION OF A COMPLIANT MECHANISM

Osman Yuksel[1], **Cetin Yilmaz***[2]

[1]Department of Mechanical Engineering, Bogazici University
osman.yuksel@boun.edu.tr

[2]Department of Mechanical Engineering, Bogazici University
cetin.yilmaz@boun.edu.tr

Keywords: Phononic Band Gap, Inertial Amplification, Compliant Mechanism, Shape Optimization, Offset Beam Element.

Abstract. *In this study, inertial amplification induced phononic gaps (stop bands) are generated using a compliant mechanism. At first, size optimization is conducted on this mechanism, to maximize stop band width and depth. Consequently, by performing shape optimization wider and deeper stop bands are obtained. To have a fast optimization process, finite element analysis is done by using one-dimensional beam elements. To check the validity of the proposed analysis scheme, a second finite element model is formed by using two-dimensional solid elements. These two finite element models yielded similar results. Then, the shape optimized mechanisms are connected in series to form one-dimensional arrays. Stop band depths of arrays with various number of unit cells (mechanisms) are compared. Moreover, the phononic band structure of the infinite periodic case is also calculated and compared with the finite periodic cases.*

1 INTRODUCTION

Phononic band gap structures have received considerable attention in the last two decades as they can be used to prevent propagation of elastic or acoustic waves in certain frequency ranges [1–3]. In the literature, both infinite and finite periodic structures are investigated. There is no wave propagation inside a phononic band gap (stop band) of an infinite periodic structure. However, there is some amount of wave propagation or vibration transmission inside the stop band of a finite periodic structure [4]. The vibration transmission amount inside the stop band is inversely proportional to the depth of the stop band in a vibration transmissibility plot. Finite periodic phononic band gap structures can be used as vibration isolation systems [5]. Therefore, if wide and deep stop bands can be obtained, these periodic structures can provide large amount of vibration isolation in wide frequency ranges.

In order to maximize the stop band width of a periodic structure, size, shape or topology optimization can be used [2, 6–8]. In size optimization, the geometry of the structure is known, but certain sizes (dimensions) of its unit cell are used as design variables. However, in shape optimization, the boundary curves/surfaces of its unit cell are either parameterized or discretized and they are varied. Whereas in topology optimization, usually the whole design domain is discretized, then the boundary curves/surfaces as well as number of holes and the location of the holes inside the design domain can be altered. In this study, both size and shape optimization methods will be utilized.

In general, phononic gaps in periodic structures are generated via Bragg scattering and local resonance methods. Refs. [4, 9] utilized mass-spring lattices to show that inertial amplification is an alternative way of generating phononic gaps, which can yield quite wide and deep stop bands at low frequencies. In this paper, this alternative method will be applied to a compliant mechanism. In compliant mechanisms, there are no rigid links or joints. The relative motions between the links are achieved through elastic deformations of the members that combine these links [10]. There are some studies that used compliant mechanisms for vibration or sound isolation [11, 12]. Moreover, there are some other studies that analyze the natural frequencies and mode shapes of compliant mechanisms [13, 14]. In this study, a bridge-type [13] compliant mechanism will be size and shape optimized to obtain a wide and deep inertial amplification induced stop band at low frequencies.

2 ANALYTICAL MODEL

In this paper, the aim is to design compliant mechanisms that can possess wide and deep inertial amplification induced stop bands at low frequencies. Before analyzing the compliant inertial amplification mechanisms via finite elements, a simple mass-spring model is investigated. In Figure 1, the two masses m are connected by a spring with stiffness k. The mass m_a and the two rigid massless links attached to this mass form the inertial amplification mechanism. The motion of the mass m_a can be obtained in terms of x, y and θ as shown in Figure 1. If θ is small, then m_a would have amplified motion when compared to the masses m. Consequently, the effective inertia of the system would be amplified [4, 9].

The equation of motion of the lumped parameter model given in Figure 1 is as follows (see Refs. [4] and [9]):

$$(m_a(\cot^2\theta + 1) + 4m)\ddot{x} + 4kx = m_a\ddot{y}(\cot^2\theta - 1) + 4ky \tag{1}$$

In Eq. 1, when y is considered as the input and x is considered as the output, the first reso-

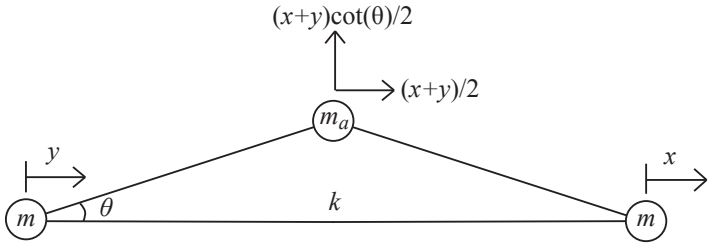

Figure 1: Lumped parameter model of the inertial amplification mechanism.

nance and antiresonance frequencies are obtained as

$$\omega_{p1} = \sqrt{\frac{k}{m + m_a(\cot^2\theta + 1)/4}} \tag{2}$$

$$\omega_{z1} = \sqrt{\frac{k}{m_a(\cot^2\theta - 1)/4}} \tag{3}$$

In Eq. 1, the numerator k denotes the static stiffness of the system, whereas the denominator denotes the dynamic mass (m_d) of the system, i.e.,

$$m_d = m + \frac{m_a(\cot^2\theta + 1)}{4} \tag{4}$$

As a result, Eq. 2 can be simplified as

$$\omega_{p1} = \sqrt{\frac{k}{m_d}} \tag{5}$$

Moreover, the static mass (m_s) of the system (see Figure 1) is

$$m_s = 2m + m_a \tag{6}$$

Note that the denominator of Eq. 3 is equal to $m_d - m_s/2$. Then, Eq. 3 can be simplified as

$$\omega_{z1} = \sqrt{\frac{k}{m_d - m_s/2}} \tag{7}$$

Once ω_{p1} and ω_{z1} are obtained, the displacement transmissibility of the system shown in Figure 1 can be written as

$$TR(\omega) = \frac{|1 - (\omega/\omega_{z1})^2|}{|1 - (\omega/\omega_{p1})^2|} \tag{8}$$

Stop band is defined as the frequency range where $TR(\omega) < 1$. Moreover, stop band depth is calculated using the highest displacement transmissibility value within the stop band. According to Eq. 8, if the excitation frequency ω is greater than ω_{z1}, then displacement transmissibility will be less than $\omega_{p1}^2/\omega_{z1}^2$. Consequently, stop band depth can be found as

$$BD = 1 - \omega_{p1}^2/\omega_{z1}^2 \tag{9}$$

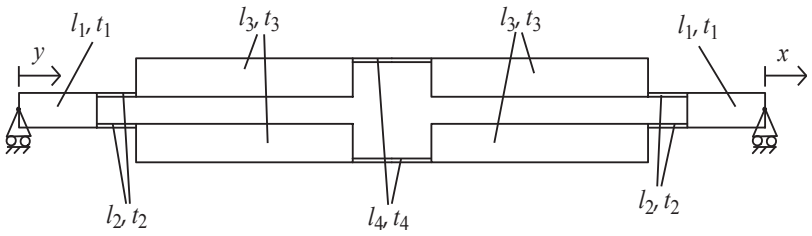

Figure 2: Compliant inertial amplification mechanism.

Hence, to increase stop band depth, one should decrease ω_{p1}/ω_{z1} ratio. For the single degree of freedom system shown in Figure 1, there is no second resonance frequency that sets an upper limit for the stop band. However, the finite element model will have multiple resonance frequencies and to have a wide stop band, the gap between the first two resonance frequencies should be maximized.

3 FINITE ELEMENT MODELS

Consider the compliant mechanism shown in Figure 2. This mechanism is formed by combining different size rectangular beams. In this figure, l_i and t_i are the length and thickness of the i^{th} beam that form the mechanism. Here, t_2 and t_4 are much smaller than t_1 and t_3. Hence, the thin beams are compliant (flexure) hinges.

Initially, finite element model of this distributed parameter system is constructed using one-dimensional offset beam elements. In order to take the offset connections of the beam elements into account, the stiffness and the mass matrices of the beam elements are multiplied with transformation matrices as in Ref. [15]. Then, a second finite element model is formed using two-dimensional solid elements for verification purposes. The beams are assumed to have large out-of-plane thickness to ensure that the deformations are in-plane. In that case, the thick beams in the model will limit the deformation of the thin beams in the out-of-plane direction, where the thin beams meet the thick beams. Thus, plane strain approximation is used in the two-dimensional finite element model.

4 STRUCTURAL OPTIMIZATION

In order to generate a wide and deep stop band at low frequencies, the compliant mechanism will be optimized. First, size optimization will be conducted to determine the optimum sizes of the rectangular beams that form the mechanism. Then, the beams with length l_3 will be shape optimized. Size and shape optimizations will be conducted using the one-dimensional finite element model to save computational time. After the optimizations, frequency response results of the two finite element models will be compared.

To obtain a wide stop band at low frequencies, the gap between the first two resonance frequencies (ω_{p1}, ω_{p2}) of the compliant mechanism should be maximized. To that end, ω_{p2}/ω_{p1} ratio will be maximized. Moreover, to obtain a deep stop band ω_{p1}/ω_{z1} ratio should be decreased (see Eq. 9).

The first two resonance frequencies of the compliant mechanism can be quickly found by modal analysis. Moreover, the first antiresonance frequency can be determined by obtaining the displacement transmissibility of the mechanism. But, to find the antiresonance frequency accurately, high frequency resolution is required, which is computationally expensive.

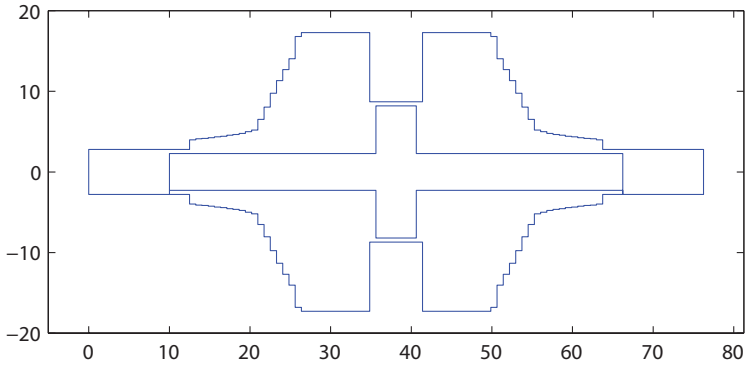

Figure 3: Shape optimized compliant mechanism that is modeled with one-dimensional beam elements.

Alternatively, the first antiresonance frequency can be quite accurately approximated by using Eq. 7. In antiresonance, the displacement characteristics of the lumped and distributed parameter models are similar. For a distributed parameter model, static stiffness (k) can be calculated with finite element method, and the system's first resonance frequency (ω_{p1}) can be obtained by modal analysis. Then, dynamic mass of the system is found by employing Eq. 5 as

$$m_d = \frac{k}{\omega_{p1}^2} \tag{10}$$

The static mass of the distributed parameter system (m_s) is equal to the summation of all individual segments of the structure. Therefore, the system's first antiresonance frequency can be found by using Eq. 7.

4.1 Size optimization

Size optimization is conducted on the compliant inertial amplification mechanism shown in Figure 2. The objective is to maximize the ratio between the second and the first natural frequencies (max ω_{p2}/ω_{p1}). The thickness of the compliant hinges (t_2 and t_4) are taken as 0.5 mm. In the first mode shape, the complaint hinges in the middle will flex twice compared to the hinges on the two ends. To have the same amount of stress in these hinges, $l_4 = 2l_2 = 5$ mm is taken as a constraint. The length l_1 and out-of-plane thickness of the mechanism b are selected as 10 mm and 20 mm, respectively. Moreover, the static stiffness of the mechanism is constrained as $k = 10^6$ N/m. Depth of the stop band is also given as a constraint, i.e., $BD = 0.2$. Finally, the material parameters are taken as $E = 210$ GPa, $\rho = 7800$ kg/m^3. The size optimization problem is solved using the Newton's method and genetic algorithm. Both methods gave the remaining free variables as $t_1 = 4.1$ mm, $l_3 = 32.2$ mm, $t_3 = 6.4$ mm.

4.2 Shape optimization

As a second step, shape optimization is performed for the beams with length l_3 of the compliant mechanism shown in Figure 2. Again, ω_{p2}/ω_{p1} ratio is aimed to be maximized with the same constraints as in the size optimization problem except that the stop band is constrained to be deeper, i.e., $BD = 0.25$. Moreover, total mass of the shape optimized mechanism is constrained to be equal to that of the size optimized one. To determine the optimum shape of the beams with length l_3, they are divided into 30 equal length segments. Besides, the thickness of these segments are allowed to vary between 0.5 mm and 15 mm. The shape optimization

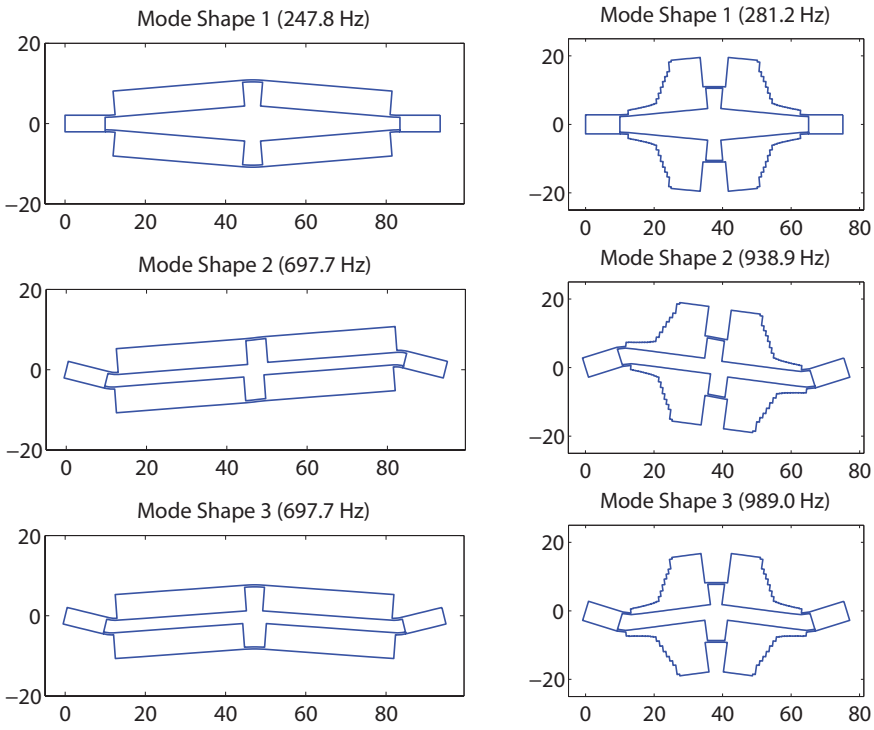

(a) (b)

Figure 4: First three mode shapes of the (a) size optimized compliant mechanism that is modeled with one-dimensional beam elements, (b) shape optimized compliant mechanism that is modeled with one-dimensional beam elements.

problem is again solved using the Newton's method and genetic algorithm. Both methods gave the following results: $t_1 = 5.6$ mm, $l_3 = 23.1$ mm. The remaining 30 thickness values that define the shape of the beams with length l_3 can be seen in Figure 3.

5 NUMERICAL RESULTS

5.1 Modal analysis

The first three mode shapes of the size and shape optimized compliant mechanisms can be seen in Figure 4. As a result of maximizing the gap between the first two resonance frequencies, the difference between the second and the third resonance frequencies is vanished for the size optimization problem. On the other hand, due to the extra mass constraint in the shape optimization problem, the second and the third resonance frequencies are not coinciding. Although stop band of the shape optimized compliant mechanism is deeper ($BD = 0.25$) compared to the size optimized compliant mechanism ($BD = 0.20$), the optimum value of ω_{p2}/ω_{p1} is also larger for the shape optimized compliant mechanism (3.34 versus 2.82). In other words, the total mass and stiffness are the same for both mechanisms, yet, the shape optimized mechanism offers a wider and deeper stop band.

5.2 Frequency response

Displacement transmissibilities of the size and shape optimized compliant mechanisms are calculated to visualize the stop bands of these mechanisms. To observe the second and third modes besides the first mode, the horizontal input displacement is placed with a small offset

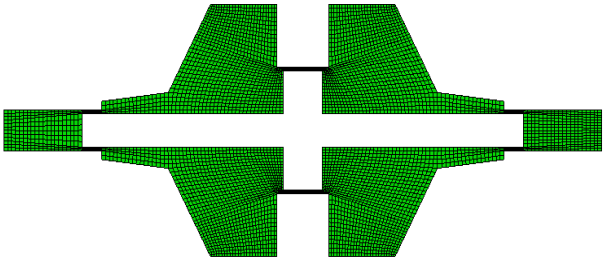

Figure 5: Shape optimized compliant mechanism that is modeled with two-dimensional solid elements.

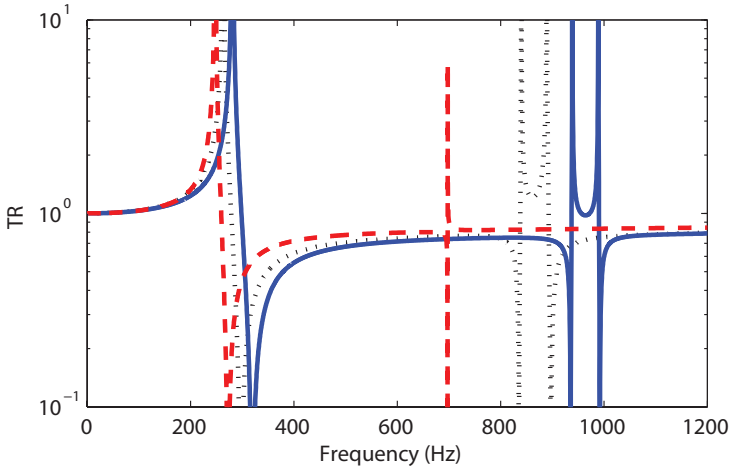

Figure 6: Displacement transmissibility plots of the size optimized compliant mechanism modeled with one-dimensional beam elements (dashed curve), shape optimized compliant mechanism modeled with one-dimensional beam elements (solid curve) and shape optimized compliant mechanism modeled with two-dimensional solid elements (dotted curve).

with respect to the centroidal axis of each mechanism. In order to check the proposed one-dimensional finite element model's validity, the shape optimized model is also simulated using two-dimensional solid finite elements. In this second finite element model (see Figure 5), the shape of the beams with length l_3 are smoothened and Poisson ratio is taken as 0.29. Displacement transmissibilities obtained by using one- and two-dimensional elements are shown in Figure 6. When the one-dimensional models of the size and shape optimized mechanisms are compared, one can see that the shape optimized mechanism offers a wider and deeper stop band. When the one- and two-dimensional models of the shape optimized mechanism are compared, it is found that the difference between the resonance frequencies can be as high as 11.5%. This difference is partly due to smoothening of the shape and partly due to element type change. However, the depth and the width of the stop band depends on ω_{p1}/ω_{z1} and ω_{p2}/ω_{p1} ratios. Moreover, the difference for the ω_{p1}/ω_{z1} ratio is about 0.5% and the difference for the ω_{p2}/ω_{p1} ratio is about 4.4%. Therefore, if the two-dimensional finite element model were used in the optimization study, similar results would be obtained.

5.3 One-dimensional array of shape optimized compliant mechanisms

The shape optimized compliant mechanism that is modeled with one-dimensional beam elements are connected in series to form one-dimensional arrays. Figure 7 shows the displacement

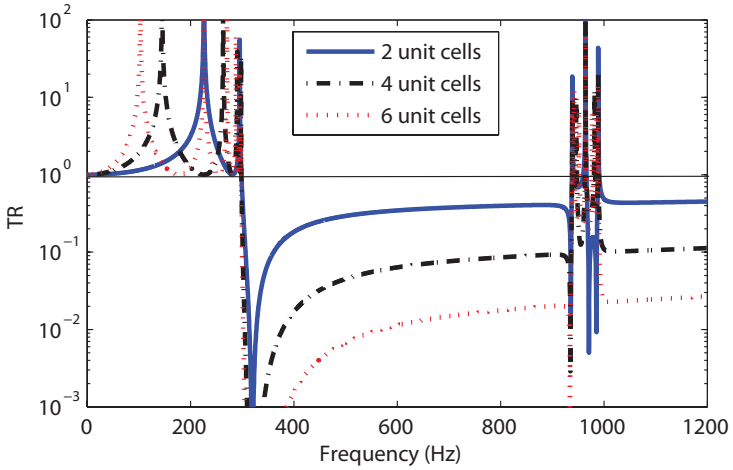

Figure 7: Displacement transmissibility plots of arrays of shape optimized compliant mechanisms that are modeled with one-dimensional beam elements.

transmissibility plots of the arrays of mechanisms that are composed of various number of unit cells (mechanisms). For two unit cells stop band depth (BD) is 0.59, for four unit cells $BD = 0.91$ and for six unit cells $BD = 0.98$. In other words, if four unit cells are used in the array only 9% of the input vibration is transmitted to the output end, whereas, if six unit cells are used in the array only 2% of the input vibration is transmitted to the output end.

Notice that, all the transmissibility plots first cross the $TR = 1$ line at the same frequency. This frequency is the lower limit of the stop band for large number of unit cells and it is denoted as ω_s. As the first resonance and antiresonance frequencies of the shape optimized compliant mechanism are much smaller than the other resonance and antiresonance frequencies, displacement transmissibility at low frequencies can be very closely approximated by Eq. 8. As a result, ω_s can be calculated by equating Eq. 8 to 1.

$$\omega_s = \sqrt{\frac{2\omega_{p1}^2\omega_{z1}^2}{\omega_{p1}^2 + \omega_{z1}^2}} \tag{11}$$

For the shape optimized mechanism ($\omega_{p1} = 281.2$ Hz, $\omega_{z1} = 319.5$ Hz), ω_s can be calculated as 298.5 Hz. Moreover, the upper limit of the stop band is $\omega_{p2} = 938.9$ Hz.

In order to investigate the limits of the lowest frequency stop band (band gap) of the infinite periodic shape optimized mechanisms, the phononic band structure (see Ref. [16]) of its unit cell should be calculated. In Figure 8, the first band gap is formed between 298.5 Hz and 938.9 Hz. Thus, Eq. 11 very well predicts the lower limit of the band gap. Moreover, the upper limit of the band gap is $\omega_{p2} = 938.9$ Hz. Therefore, the stop band limits of the finite and infinite periodic cases match.

6 CONCLUSIONS

In this paper, size and shape optimizations are conducted on a compliant mechanism to obtain wide and deep stop bands. In order to maximize the stop band width and depth of the mechanism, its first two resonance frequencies and its first antiresonance frequency are calculated with the use of one- and two-dimensional finite element models. It is shown that both finite element models give similar stop band width and depth values. As the one-dimensional finite element model is faster solve, it is used for size and shape optimizations of the compliant

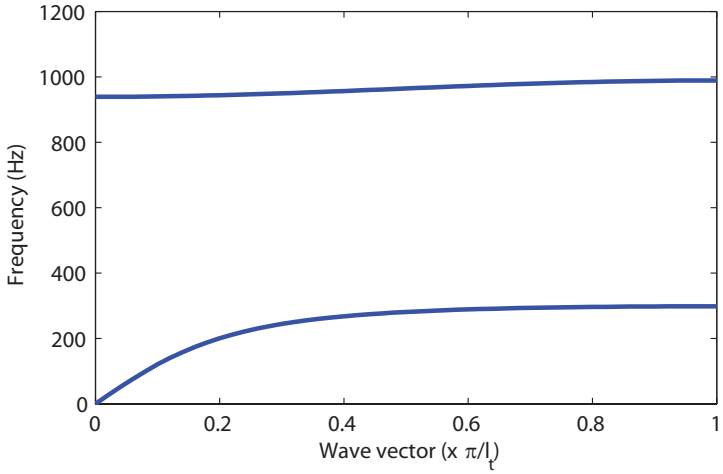

Figure 8: Phononic band structure of the infinite periodic shape optimized mechanism that is modeled with one-dimensional beam elements. Here, l_t denotes the length of the mechanism.

mechanism. When size and shape optimized compliant mechanisms are compared, it is seen that the shape optimized mechanism offers both a wider and deeper stop band. Then, the shape optimized compliant mechanisms are connected in series to form one-dimensional arrays. It is shown that quite deep stop bands can be achieved with few number of unit cells (mechanisms). Finally, the phononic band structure of the infinite periodic compliant mechanism is obtained and it is seen that the stop band frequency range of this case is very similar to the finite periodic cases.

ACKNOWLEDGEMENTS

This work was supported by TUBITAK Grant No. 110M663.

REFERENCES

[1] M.M. Sigalas and E.N. Economou, Elastic and acoustic wave band structure. *Journal of Sound and Vibration*, **158**, 377–382, 1992.

[2] O. Sigmund and J.S. Jensen, Systematic design of phononic band–gap materials and structures by topology optimization. *Philosophical Transactions of the Royal Society of London. Series A: Mathematical, Physical and Engineering Sciences*, **361**, 1001–1019, 2003.

[3] A. Khelif, B. Aoubiza, S. Mohammadi, A. Adibi and V. Laude, Complete band gaps in two-dimensional phononic crystal slabs. *Physical Review E*, **74**, 046610, 2006.

[4] C. Yilmaz and G.M. Hulbert, Theory of phononic gaps induced by inertial amplification in finite structures. *Physics Letters A*, **374**, 3576–3584, 2010.

[5] J. Wen, G. Wang, D. Yu, H. Zhao and Y. Liu, Theoretical and experimental investigation of flexural wave propagation in straight beams with periodic structures: Application to a vibration isolation structure *Journal of Applied Physics*, **97**, 114907, 2005.

[6] H.F.D. Policarpo, O.M. Silva and M.M. Neves, An eigenfrequency approach to characterize and optimize 1D two material structures for axial vibration attenuation. *International Conference on Mathematics and Continuum Mechanics*, 41–52, 2008.

[7] A.S. Knudsen, Design of stop-band filters by use of compound curved pipe segments and shape optimization. *Structural and Multidisciplinary Optimization*, **44**, 863-874, 2011.

[8] N. Olhoff, B. Niu and G. Cheng, Optimum design of band-gap beam structures. *International Journal of Solids and Structures*, **49**, 3158–3169, 2012.

[9] C. Yilmaz, G.M. Hulbert and N. Kikuchi, Phononic band gaps induced by inertial amplification in periodic media. *Physical Review B*, **76**, 054309, 2007.

[10] L.L. Howell, *Compliant Mechanisms*. Wiley, New York, 2001.

[11] T. Tantanawat, Z. Li and S. Kota, Application of compliant mechanisms to active vibration isolation systems. *International Design Engineering Technical Conference, Proceedings of DETC 2004*, 1–8, 2004.

[12] E.M. Dede and G.M. Hulbert, Analysis, design, and optimization of structures with integral compliant mechanisms for mid-frequency response. *International Journal for Numerical Methods in Engineering*, **73**, 470–492, 2008.

[13] H.W. Ma, S.M. Yao, L.Q. Wang and Z. Zhong, Analysis of the displacement amplification ratio of bridge-type flexure hinge. *Sensors and Actuators A*, **132**, 730–736, 2006.

[14] Q. Xu and Y. Li, Analytical modeling, optimization and testing of a compound bridge-type compliant displacement amplifier. *Mechanism and Machine Theory*, **46**, 183–200, 2011.

[15] R.E. Miller, Dynamic aspects of the error in eccentric beam modeling. *International Journal for Numerical Methods in Engineering*, **15**, 1447–1455, 1980.

[16] L. Brillouin, *Wave propagation in periodic structures: electric filters and crystal lattices*. Dover, New York, 1953.